Dalton Transactions

ROYAL SOCIETY OF CHEMISTRY

PAPER

View Article Online
View Journal | View Issue

Cite this: *Dalton Trans.*, 2024, **53**, 7376

Preparation of monodisperse cerium oxide particle suspensions from a tetravalent precursor†

Ashley M. Hastings, [a] Susana Herrera,[b,c] Sharee Harris, [d] Tashi Parsons-Davis, [a] Andrew J. Pascall [e] and Jennifer A. Shusterman *[a]

Received 17th January 2024,
Accepted 29th March 2024

DOI: 10.1039/d4dt00146j

rsc.li/dalton

Cerium oxide particles are a unique material that enables studying the intersection of metal oxides, *f*-elements, and nanomaterials. Distinct from diverse applications in catalysis, energy, and medicine, cerium possesses additional influence as a non-radioactive actinide surrogate. Herein, we present a synthesis for sub-micron cerium particles using hexamethylenetetramine and ammonium hydroxide as precipitating agents with a Ce^{IV} precursor. The combinatorial homogeneous precipitation approach yields monodisperse and moderately-stable CeO_2 particle suspensions in ethanol, as determined by powder X-ray diffraction, scanning electron microscopy, dynamic light scattering, and zeta potential measurements. Various additives may be used to moderate and manipulate the surface charge of the particles. Proof-of-concept electrophoretic deposition of the particles produces a uniform layer of CeO_2 on graphite. The synthesis and suspension properties are developed as a methodology towards future controlled actinide hydrolysis and film deposition.

Introduction

Ceria (CeO_2) offers enhanced functionality over other ceramics because of its opportunistic redox properties ($Ce^{III/IV}$) and the interplay of 5*d* and 4*f* electrons and vacancies.[1,2] The phase is often described as the substoichiometric CeO_{2-x}, to reflect the ability of surface Ce atoms to toggle between Ce^{IV} and Ce^{III} in the lattice.[3] This fundamental reactivity of ceria is inherently based at the surface of the material.[4] One method to increase the accessible surface area, and thereby increase reactivity, is to decrease the particle size into the nanoscale. Furthermore, nanoparticles display unique physical and chemical properties over that of the bulk material.[3] Cerium nanoparticles (Ce NPs) have demonstrated widespread use in heterogeneous catalysis and energy applications, including hydrogen generation, fuel cells, and photocatalytic water splitting.[2,3,5,6] More recently, Ce NPs are proving to be promising candidates in many biomedical applications, including antioxidants, drug delivery, and tissue engineering.[7,8]

Our interest in Ce NPs is as an actinide surrogate for use in additive manufacturing (AM). Cerium is commonly used as a stable surrogate for trivalent and tetravalent actinides in the nuclear field. The actinides (*e.g.*, Th, U, Np, Pu) offer similar reactivity to Ce, albeit with 6*d* and 5*f* orbitals and even more exotic redox character.[9–11] While Ce^{III} is stable in solution, trivalent U, Np, and Pu in solution are transient.[11] Furthermore, while trivalent U, Np, and Pu exist, the higher valent cations are more stable in oxic conditions.[12] Actinide nanoparticles, particularly for Np and Pu, have largely been explored in the context of intrinsic colloid formation, typically formed unintentionally.[13–15] Pu nanoparticle formation is often irreversible and results in small particles <5 nm in size.[16–18] We are investigating the controlled synthesis of large nanoparticles (*i.e.*, ~100 nm in diameter) for use in AM of metal oxide films. Nanoparticle feedstocks for AM may offer the solutions to several challenges with existing actinide deposition technologies and introduce additional functionalities.[19] Currently, increasing deposit thickness can compromise layer homogeneity and integrity.[20] We propose that by using large spherical nanoparticles, AM feedstocks can increase metal content without sacrificing deposit uniformity. While reports of Ce nano- to sub-micron particle syntheses are abundant, none are readily deployable for the practicalities of transuranic work, which requires scale minimization, radiological manipulation limitations, and use of acidic stock solutions. To initiate this investigation, we developed an alternative synthesis leveraging a Ce^{IV} precursor for the assembly of CeO_2 particles which can better represent actinide systems.

[a]*Nuclear and Chemical Sciences Division, Lawrence Livermore National Laboratory, Livermore, CA 94550, USA. E-mail: shusterman1@llnl.gov*
[b]*Florida International University, Miami, FL 33199, USA*
[c]*Pacific Northwest National Laboratory, Richland, WA 99352, USA*
[d]*Materials Science Division, Lawrence Livermore National Laboratory, Livermore, CA 94550, USA*
[e]*Materials Engineering Division, Lawrence Livermore National Laboratory, Livermore, CA 94550, USA*

† Electronic supplementary information (ESI) available. See DOI: https://doi.org/10.1039/d4dt00146j

Ce NPs may be synthesized by a "top down" (*i.e.*, mechanical milling of bulk oxide powders) or "bottom up" (*i.e.*, hydrolysis of metal ions in solution) approach to achieve the desired size and properties.[21] Thermal treatment is also a common pathway to convert to oxides, remove assisting ligands, or otherwise sinter the oxide products.[22–25] Solution-based syntheses are attractive because they limit dispersibility and include a variety of diverse approaches: precipitation, sol–gel, sonochemical, microwave-assisted, and hydro-/solvothermal methods.[21] Across these synthetic pathways, Ce^{III} precursors are almost exclusively used to produce $Ce^{IV}O_2$ nanoparticles, relying on *in situ* oxidation.[1,24,26–37] Some exceptions to this are hydrothermal synthesis reports by Hsu *et al.*[38] and Panahi-Kalamuei *et al.*[39] that used Ce^{IV} sulfate and ammonium Ce^{IV} nitrate precursors, respectively. The dominance of Ce^{III} precursors is unsurprising given its favorable solubility in various reaction media, compared to Ce^{IV}. Tetravalent metals generally have lower solubilities than trivalent metals and are known to readily form intractable hydrolysis products.[12,40] Such hydrolytic mechanisms, however, are necessary for solution-based oxide nanoparticle formation but must occur in a controlled manner. Manual additions of ammonium hydroxide to a Ce^{IV} solution yields precipitation with little control over particle size and morphology because of the rapid and localized introduction of the base.[24] Homogeneous precipitation (also known as coprecipitation) relies on the *in situ* generation of the precipitating agent to raise the pH uniformly and allow hydrolysis reactions to proceed, resulting in more uniform and size-tunable particle growth.[24]

Herein, we present a modification of several previously-reported homogeneous precipitation approaches.[1,24,26] Hexamethylenetetramine (HMT) is a common alkalizer in homogeneous precipitation reactions as it decomposes to form ammonia.[1,24,41] Chen and Chen originally reported an aqueous Ce NP synthesis with Ce^{III} nitrate, HMT, and mild heating.[24] Zhang *et al.*[26] and Parimi *et al.*[1] prepared Ce NPs with the same reaction constituents, but at room temperature. Our approach relies on the combination of HMT and ammonium hydroxide for the room-temperature assembly of Ce particles in a mixed water and ethanol reaction solution. We selected a bulk CeO_2 precursor dissolved in nitric acid, in the style of an actinide stock solution. The resulting particle suspensions are studied for size, dispersity, and suspension stability as a function of pH adjustment, aging time, and steric-stabilizing additives. Electrophoretic deposition[42,43] of the Ce particles exhibits the homogeneity that can be accessible with sub-micron particle feedstocks for additive manufacturing.

Experimental

Materials

Cerium dioxide (Fisher Scientific), nitric acid (ACS Reagent, 70%, Sigma Aldrich), ethanol (200 proof, anhydrous, PHARMCO), hexamethylenetetramine (HMT) (99+%, Thermo Scientific), ammonium hydroxide (30–33% NH_3 in H_2O, Sigma Aldrich), acetylacetone (≥99%, Sigma Aldrich), Darvan 821-A (Vanderbilt Minerals, Inc.), polyethyleneimine (PEI) (branched, 800 MW, Sigma Aldrich), urea (ACS Reagent, 99.0–100.5%, Sigma Aldrich), citric acid (ACS Reagent, ≥99.5%, Sigma Aldrich) were used as received. Circular, 8 mm discs were punched out of 0.5 mm graphite foil (99.8%, Alfa Aesar). Milli-Q water (18.2 MΩ cm at 25 °C) was the water source.

Methods

Synthesis. A 0.58 M Ce^{IV} stock solution was prepared by dissolving CeO_2 in concentrated HNO_3 (15.8 M) under mild heating. A 0.12 M Ce^{IV} working solution was then prepared by a 1 : 4 dilution with 0.5 M HNO_3, to a final acid concentration of 3.56 M HNO_3. To a 20 mL glass scintillation vial, 5 mL of both H_2O and EtOH were pre-equilibrated with stirring at 800 rpm for 5 minutes. HMT was freshly dissolved in 1 : 1 H_2O/EtOH to yield a 0.41 M HMT solution. The HMT (1 mL) was added to the reaction flasks and stirred for at least 5 minutes. Then, 0.667 mL of the 0.12 M Ce working solution was added to the flasks to produce an intense orange solution. Over the course of 10–15 minutes of stirring, the reaction solution changed to a pale-yellow color. The pH of the reaction solution was adjusted with 30–33% NH_4OH to the desired synthesis pH ($1.5 < pH < 7.5$). The increase in pH caused particle formation, which was evident by the solutions becoming off-white and cloudy. The solutions were aged at room temperature overnight with stirring at 800 rpm. The Ce particles were harvested using centrifugation and washed three times with ethanol. Ultrasonication was used to disperse particles in each round of fresh solvent. This was executed in a Q500 QSonica system with a cup horn attachment (typically two 30 s rounds at 50% amplitude). In order to achieve well dispersed suspensions, thorough washing was necessary to remove unreacted synthesis components. Incomplete washing (*e.g.*, only 1 round of ethanol instead of 3) yielded aggregated suspension. The particle batches were stored as ethanol suspensions to minimize dispersibility hazards. Syntheses at twice of the above-stated reaction scale conducted in 50 mL glass round bottom flasks were also successful but tended to have higher polydispersity indexes (0.15–0.17) for the resulting Ce particle suspensions.

Powder X-ray diffraction. Cerium particles were dropcast onto zero-background Si wafers from an ethanol suspension. Powder diffractograms were collected on a Bruker D8 Advance diffractometer outfitted with a Cu X-ray tube and a LynxEye detector. The data range was 20–80° 2θ with 0.02° steps and 3 s collections per step. Samples were rotated. A divergence slit of 0.6 mm and an antiscattering slit of 2 mm were used. Cu Kα2 contributions were subtracted from the patterns.

Dynamic light scattering (DLS) and zeta potential. Particle batch suspensions were ultrasonicated to homogenize the dispersion, diluted in ethanol (*e.g.*, 10–40 μL added to 1 mL EtOH), ultrasonicated again, and transferred to DTS1070 folded capillary cells. The spike aliquot of each batch was adjusted to optimize scattering intensity for the DLS measurement. The samples were immediately run on a Malvern

Zetasizer Ultra in triplicate cycles for the size regime and 1–3 cycles for the zeta potential measurements. Error in these measurements is reported as 2σ for averaged replicates. For the additive study, each additive was combined with a 100 μL homogeneous aliquot of the Ce particle batch and ultrasonicated. Quantities are provided in Table S5.† Then, 20 μL of these suspensions were diluted with ethanol for the DLS and zeta potential measurements as previously described.

Scanning electron microscopy. Particles were deposited onto aluminum stubs from recently ultrasonicated ethanolic suspensions. The samples were carbon-coated using a Quorum 150T ES sample coater. Micrographs were obtained from an FEI Inspect F scanning electron microscope with an Everhart–Thornley detector and an operating voltage of 15–20 kV. ImageJ software was used to estimate particle size.[44] With the size of these particles approaching the resolution limits of the available instrumentation, we selected 100 particles with at least 2/3 of the particle boundary visible.

Electrophoretic deposition (EPD). Ce particles were deposited under similar conditions as a previously reported procedure.[45,46] Briefly, our 3D printed EPD cell (Formlabs clear resin) was outfitted with stainless steel electrodes. Graphite foils were loaded onto the negative electrode. Particle batches synthesized at pH ~4.5 were diluted to ~1.5 mL with ethanol and freshly ultrasonicated before deposition. Particle suspensions were flowed by syringe pump (1 mL min^{-1}), back-and-forth two times, through the chamber with an applied potential of 200 V. After disassembling the cell, EPD green bodies were allowed to air dry before being calcined at 500 °C for 1.5 hours.

Results and discussion

Homogeneous precipitation

We employed a dual-alkalizer approach with HMT and ammonium hydroxide for homogeneous precipitation of cerium particles from a Ce^{IV} precursor. The Ce^{IV} is pre-equilibrated with HMT to moderate the particle growth and maintain the Ce oxidation state; the ammonium hydroxide is added manually to counteract the acidity of the Ce^{IV} stock, dictated by the Ce^{IV}'s solubility, and accelerate hydrolytic mechanisms. The initial formation of Ce particles is evident during the pH-adjusting phase of the synthesis (Fig. 1A and Fig. S1†). Before any base addition, the pH of the reaction solution is approximately 1. At and above a pH of 1.5, the reaction solution begins to look cloudy from the particle nucleation. Increases in pH achieve further particle nucleation, but if the pH increases above 8, then precipitation of an amorphous cerium hydroxide phase competes with the controlled Ce particle formation. The precipitate readily settles out of suspension, in contrast with the more uniform particles, which generally remain suspended in the reaction solution. After the ammonium hydroxide addition, the HMT continues to hydrolyze and acts as an additional source of ammonium hydroxide if the adjusted reaction solution pH is less than 5.5 (Fig. 1B).

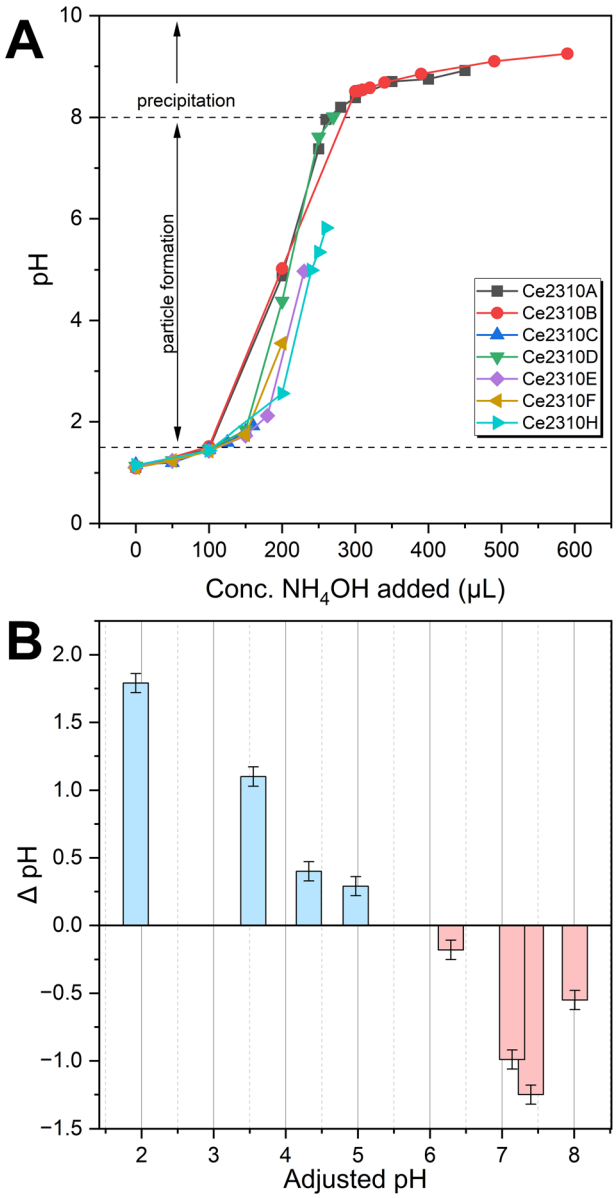

Fig. 1 (A) Titration curves for several Ce particle reaction solutions. Error is contained within the data points. No initial particle formation is observed for pH < 1.5. (B) The change in pH of reaction solutions after ~18 hours of aging as a function of the synthesis pH from adjustment with NH_4OH. The error is 0.05 for pH measurements.

This result agrees with previous findings regarding the decomposition of HMT.[24] With reaction solutions that have a pH above 6, HMT decomposition is less dominant, but the extent of hydrolysis leads to increased consumption of OH^- from solution by olation/oxolation reactions of cerium and the particle nucleation.[9] Hence, the reaction solution pH decreases with aging overnight.

Solid-state characterization

The Ce powders are consistent with the nanocrystalline CeO_2 fluorite structure, by powder X-ray diffraction (Fig. 2A) on a

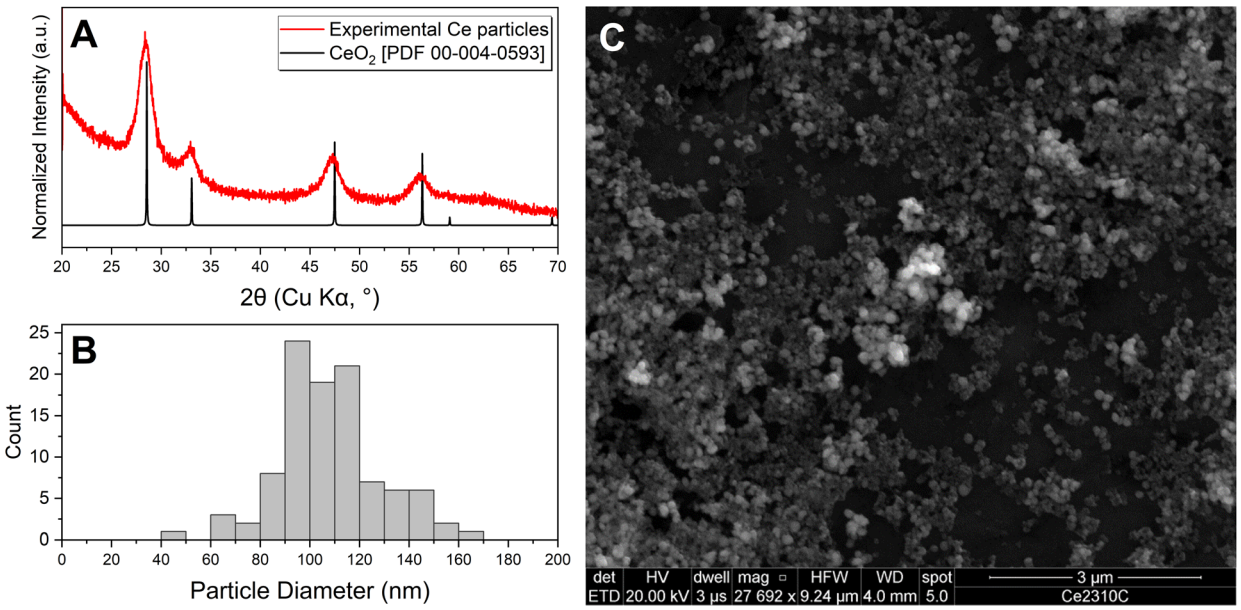

Fig. 2 (A) Powder X-ray diffraction on the cerium particles. (B) Particle size analysis conducted on (C) the scanning electron micrograph of cerium particles.

batch synthesized at pH 7.4. The cubic lattice consists of 8-coordinate Ce metal centers with square prismatic geometry and tetrahedrally coordinated oxygen atoms. The broad Bragg peaks are characteristic of nanomaterials.[47] Scanning electron micrographs (Fig. 2C) on a pH 1.9 batch reveal particles of medium-to-high sphericity, with some particles exhibiting more ellipsoidal morphology by qualitative observation. The particles form irregular agglomerates when concentrated on the aluminum stub. Edge-to-edge bisecting lines of particles through ImageJ analysis yield approximate particle diameters (Table S1†). The average particle size is 108 ± 41 nm and Fig. 2B shows the resulting distribution. While we were aiming for large nanoparticles, these particles are in the sub-micron size regime because the average diameter is greater than the 100 nm cutoff for nanoparticles.

Suspension behavior

After proper washing and dispersion through ultrasonication, ethanolic Ce particle suspensions were characterized by dynamic light scattering and zeta potential measurements. The suspensions are monomodal and show hydrodynamic diameters of ~60–200 nm, according to volumetric distributions (Fig. 3). The intensity distributions reveal Z_{avg} of 115–175 nm (Fig. S4 and Table S2†). Increasing the pH of the synthesis reaction solution does not change the resulting hydrodynamic diameter of the particles, however there can be some size variability as seen in the pH 3.6 batch as compared to pH 1.9, 5.0 and 6.3. Batch-to-batch variation can occur because the localized introductions of NH_4OH during the pH adjusting step affects the particle nucleation. HMT controls the ripening of the particles as the reaction solution ages overnight so that the resulting particle size distribution is mostly narrow and

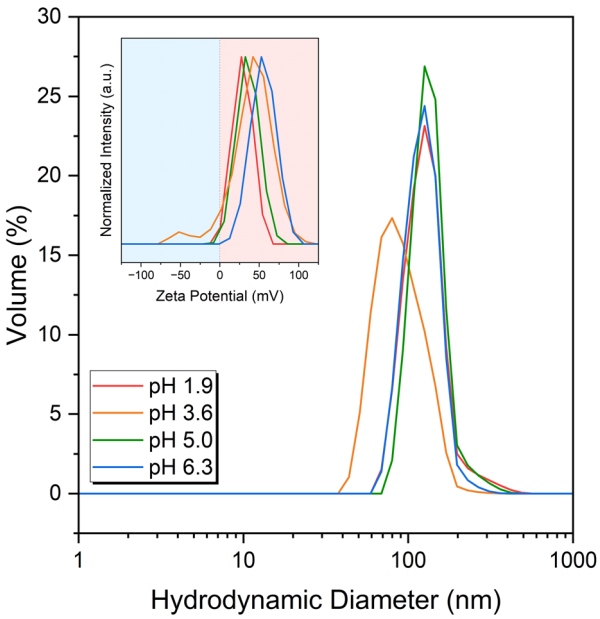

Fig. 3 Dynamic light scattering volume distributions of Ce particle batches synthesized at the indicated pHs. Inset are the corresponding zeta potential measurements.

can be described as monodisperse, because the polydispersity index (PDI) is <0.1 (Table S2†).[48] The pH 3.6 batch has a PDI of 0.112 ± 0.023, just over the threshold into moderate polydispersity. The number-derived hydrodynamic diameter agrees with the particle size distribution from SEM (Fig. S5†). The slight shift to higher diameters for the hydrodynamic volume and intensity distributions as compared to solid-state measurements is a known bias for DLS.[29,34] The overall

agreement between the hydrodynamic diameters and the particle size as evaluated from SEM indicates successful dispersion of the particles in suspension. Recharacterization after 1–2 weeks reveals consistency after aging (Fig. S6 and Table S3†) although there may be a ripening effect of the pH 3.6 batch, which has a ~10% increase in Z_{avg}. Additionally, most show a reduction in PDI, although these are still within 2σ error (Table S4†). The consistency of the feedstock characteristics, at least in the short term, enhances its utility because batches can be prepared in advance of their use. These suspensions have positive zeta potentials of 25–55 mV, indicating moderate-to-good stability (Fig. 3),[49] and are consistent with, if not more stable than previous reports.[1,29,34] Generally, particles with higher charged surfaces (if it is the same sign) electrostatically repel each other to yield more stable suspensions. Here we use the word "stable" to describe monodisperse, unaggregated suspensions that are resistant to settling. We have observed a range of gravitational sedimentation behavior of these particles, likely driven by the concentration of the suspension (Fig. S7†). More concentrated suspensions have increased particle-particle interactions that can lead to sedimentation, in as few as 15 minutes. Less concentrated suspensions, however, remained dispersed across several days. While not studied further herein, suspension aging and particle concentration are other parameters that can be tuned to optimize the Ce particle characteristics relative to bulk CeO_2 powders.

Aggregation phenomena in some of our particle batches manifest as multiple populations as well as shifting to much higher hydrodynamic diameter (*e.g.*, ~1000 nm) in the DLS results. Even in samples where the particles appear monodisperse in the intensity distribution, it is important to check the volume distribution, which can reveal a more complicated suspension behavior (Fig. S8†). Such disparity can arise between the intensity, volume, and number distribution plots as the intensity plots are closest to what is actually measured and are skewed by larger particles ($I \propto 10^6 \times d$, where d is particle diameter).[50,51] Volume and number distributions require suitable data quality and several assumptions (*i.e.*, spherical particles, homogeneous particle density, and known refractive index) to transform the intensity data.[52] Results from PXRD and SEM support these assumptions in our case. See Fig. S5† as an example of how intensity, volume, and number distributions compare for the same sample. In our Ce particle system, such aggregation effects can be mitigated by proper washing to remove unreacted synthesis components and with proper ultrasonication.

Additives are often used to stabilize particle suspensions and/or induce additional functionality.[28,34,43,53] We screened the effects of acetylacetone (acac), Darvan 821-A, polyethyleneimine (PEI), water, urea, and citric acid on our Ce particle suspensions (Fig. 4). There can be some inherent variation in DLS and zeta potential measurements as can be seen in the Control 1 and Control 2 samples in Fig. 4A, which were measured on different aliquots from the same batch at the beginning and end of the experiment session, respectively. Largely, the hydrodynamic diameters of the particles investigated with the additives were unchanged from the plain Ce particle batch, except for citric acid, which shows an increase in Z_{avg} (Table S6†). The zeta potential measurements reveal modifications to the particle surface charges. The addition of aqueous citric acid destabilized the suspension by an ~80% reduction in zeta potential to +9.19 ± 1.43 mV. The citrate

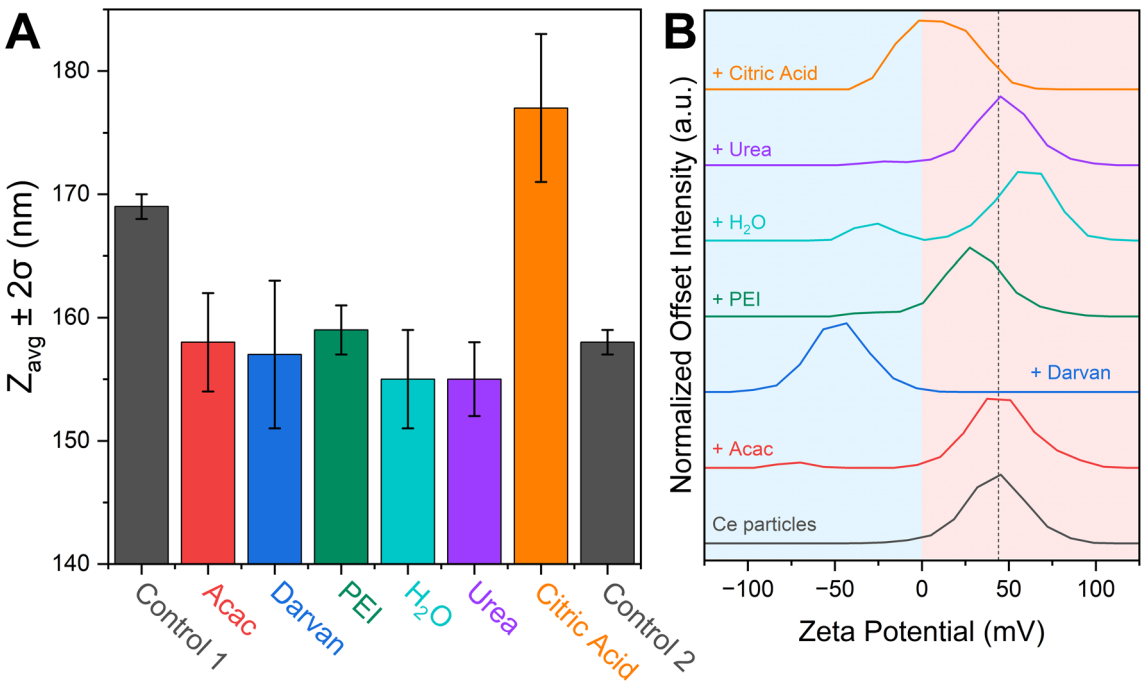

Fig. 4 The effect of the indicated additives on a batch of Ce particles on (A) Z_{avg} and (B) zeta potential measurements.

anions were electrostatically attracted to the positive Ce particle surfaces and upon association, neutralized most of the surface charge. This result contrasts with a previous report of citric acid's effectiveness as a surfactant for Ce nanoparticles, but those particles had negative to near neutral initial surface charges.[34] PEI also reduces the suspension zeta potential by ~30%, which is still within range of what we have observed for these Ce particles, but urea and acac maintain the positive surface charge. Darvan 821-A, produced zeta potentials of similar magnitude but opposite charge. Darvan 821-A is a common dispersing agent for ceramic particles and is made of ammonium polyacrylate. Like citrate, it is ionic in solution, but introduces a steric bulk for stabilization. Charge flipping on the particles could be useful in electrical applications, and negatively-charged CeO_2 particles have a greater precedent in therapeutic agents;[54] however, some optimization would be necessary as the viscous additive was not fully miscible with the ethanolic suspension. Since urea and citric acid were introduced as aqueous spikes, we conducted an experiment with a water spike as a control. Interestingly, water as an additive produces a bimodal zeta potential distribution with negative (−27.4 ± 4.8 mV) and positive (+56.4 ± 7.1 mV) populations, with no evidence of aggregation in the DLS data (Fig. S9 and S10†). With the negative population accounting for ~17% of the integrated intensity, the overall suspension zeta potential averages to +45.0 ± 2.4 mV with water present. Even as a minor component, water introduces proton exchange reactions with the surface of particles.[53] The dissociation of water into $H^{\bullet}$ and $OH^{\bullet}$ radicals is known to occur from ultrasonication and the sonochemical reaction progresses further in alcohol/water mixtures than either of the independent solvents.[55] As the water control produced a distinct zeta potential feature, we can conclude that the effects of the urea and citric acid additives are indeed ligand-based and not solely a result of introducing water to the system.

Electrophoretic deposition

To demonstrate the potential of these Ce particle suspensions as AM feedstocks, Ce layers were coated onto graphite backings through electrophoretic deposition. The positively-charged Ce particles deposited onto negatively-charged electrodes. Optical microscopy reveals relatively uniform and crack-free coatings of CeO_2 after calcination at 500 °C (Fig. 5). Any heterogeneous features arise from existing texture in the graphite foil. In contrast, Panigrahi *et al.*,[53] reported uneven surfaces on ceria EPD deposits from ethanol, but their commercial CeO_2 particles were larger, up to 3 μm in size. We have shown preliminary evidence that our narrow size range Ce particles can improve the microstructure of Ce EPD deposits. Optimization and tuning of the deposition conditions are underway.

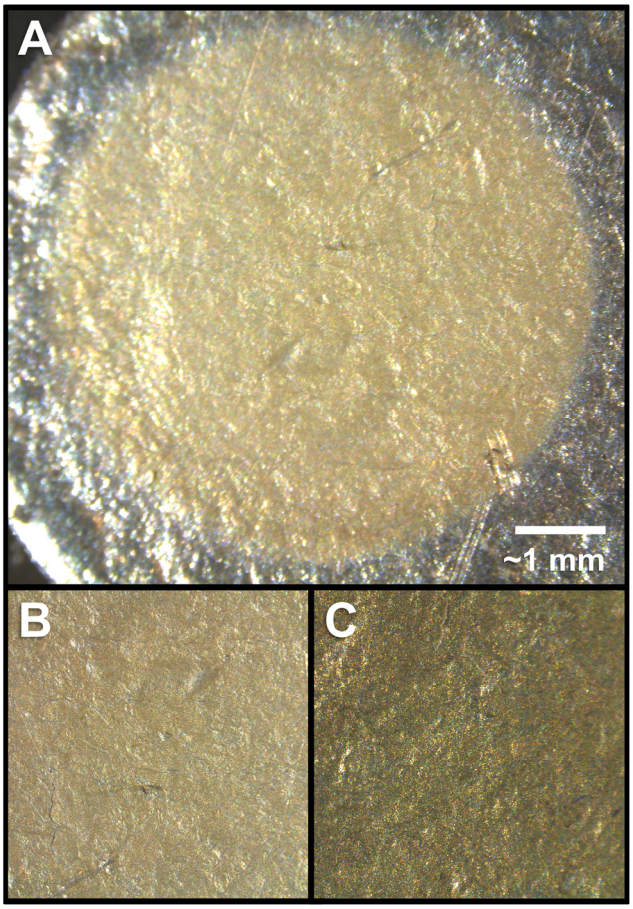

Fig. 5 Optical microscope images of calcined Ce deposits on a graphite backing with magnifications of (A) 1.25×, (B) 2.5×, and (C) 8×.

Conclusions

We report a simple synthesis for sub-micron Ce particles from a tetravalent precursor that is tuned towards application to tetravalent actinides. The combination of HMT and ammonium hydroxide produces controlled particle precipitation at room temperature. The method yields particles of a favorable size (~60–200 nm) for an additive manufacturing feedstock; the particles are monodisperse and large enough so that the product is recoverable by standard centrifugation, yet not so large as to readily settle out of ethanolic suspensions. This presents a marked improvement over typical actinide colloid suspensions, which are notorious for being difficult to harvest and wash for further use due to their small size. The Ce particles have positive surface charge which can be modified by the introduction of various additives (*e.g.*, Darvan 821-A for charge flipping). Early progress demonstrates the efficacy of these Ce particle feedstocks for producing uniform films by electrophoretic deposition. This work serves as the foundation for the synthesis of spherical sub-micron transuranic oxide particles, pending ongoing scaling procedures and optimization appropriate for high activity alpha-emitting radionuclides.

Author contributions

Ashley M. Hastings: investigation, validation, visualization, and writing – original draft; Susana Herrera: investigation and

methodology; Sharee Harris: investigation; Tashi Parsons-Davis: supervision; Andrew J. Pascall: resources and supervision; Jennifer A. Shusterman: conceptualization, funding acquisition, resources, supervision, and writing – review & editing.

Conflicts of interest

The authors have no conflicts of interest to declare.

Acknowledgements

This work was performed under the auspices of the U.S. Department of Energy by Lawrence Livermore National Laboratory under Contract DE-AC52-07NA27344. This work was supported by Laboratory Directed Research and Development project 23-FS-010. S. Herrera was funded by the NNSA Graduate Fellowship Program. We are grateful to LLNL's Glenn T. Seaborg Institute for access to their Zetasizer.

References

1 D. Parimi, V. Sundararajan, O. Sadak, S. Gunasekaran, S. S. Mohideen and A. Sundaramurthy, *ACS Omega*, 2019, **4**, 104–113.
2 R. M. Pallares and R. J. Abergel, *Nanoscale*, 2020, **12**, 1339–1348.
3 D. Zhang, X. Du, L. Shi and R. Gao, *Dalton Trans.*, 2012, **41**, 14455.
4 J. Huang, Y. Yu, J. Zhu and R. Yu, *Sci. China: Technol. Sci.*, 2018, **61**, 135–139.
5 M. Melchionna and P. Fornasiero, *Mater. Today*, 2014, **17**, 349–357.
6 M. C. Wasson, X. Zhang, K. Otake, A. S. Rosen, S. Alayoglu, M. D. Krzyaniak, Z. Chen, L. R. Redfern, L. Robison, F. A. Son, Y. Chen, T. Islamoglu, J. M. Notestein, R. Q. Snurr, M. R. Wasielewski and O. K. Farha, *Chem. Mater.*, 2020, **32**, 8522–8529.
7 N. Thakur, P. Manna and J. Das, *J. Nanobiotechnol.*, 2019, **17**, 84.
8 H. Li, P. Xia, S. Pan, Z. Qi, C. Fu, Z. Yu, W. Kong, Y. Chang, K. Wang, D. Wu and X. Yang, *Int. J. Nanomed.*, 2020, **15**, 7199–7214.
9 A. Ikeda-Ohno, C. Hennig, S. Weiss, T. Yaita and G. Bernhard, *Chem. – Eur. J.*, 2013, **19**, 7348–7360.
10 J. G. Darab, H. Li, J. J. Bucher, J. P. Icenhower, P. G. Allen, D. K. Shuh and J. D. Vienna, *J. Am. Ceram. Soc.*, 2022, **105**, 6627–6639.
11 *The Chemistry of the Actinide and Transactinide Elements*, ed. L. R. Morss, N. M. Edelstein and J. Fuger, Springer, Dordrecht, The Netherlands, 4th edn, 2010.
12 K. E. Knope and L. Soderholm, *Chem. Rev.*, 2013, **113**, 944–994.
13 H. Itagaki, S. Tanaka and M. Yamawaki, *Radiochim. Acta*, 1991, **52–53**, 91–94.
14 P. Zhao and S. A. Steward, *Literature review of intrinsic actinide colloids related to spent fuel waste package release rates*, Lawrence Livermore National Laboratory, Livermore, CA, 1997.
15 R. Husar, R. Hübner, C. Hennig, P. M. Martin, M. Chollet, S. Weiss, T. Stumpf, H. Zänker and A. Ikeda-Ohno, *Chem. Commun.*, 2015, **51**, 1301–1304.
16 D. Hudry, C. Apostolidis, O. Walter, A. Janßen, D. Manara, J.-C. Griveau, E. Colineau, T. Vitova, T. Prüßmann, D. Wang, C. Kübel and D. Meyer, *Chem. – Eur. J.*, 2014, **20**, 10431–10438.
17 C. Ekberg, K. Larsson, G. Skarnemark, A. Ödegaard-Jensen and I. Persson, *Dalton Trans.*, 2013, **42**, 2035–2040.
18 E. Dalodière, M. Virot, V. Morosini, T. Chave, T. Dumas, C. Hennig, T. Wiss, O. Dieste Blanco, D. K. Shuh, T. Tyliszcak, L. Venault, P. Moisy and S. I. Nikitenko, *Sci. Rep.*, 2017, **7**, 43514.
19 M. Rahman, K. S. Islam, T. M. Dip, M. F. M. Chowdhury, S. R. Debnath, S. Md. M. Hasan, Md. S. Sakib, T. Saha, R. Padhye and S. Houshyar, *Prog. Addit. Manuf.*, 2023, DOI: 10.1007/s40964-023-00514-8.
20 J. B. Roberto, M. Du, J. G. Ezold, S. L. Hogle, J. Moon, K. Myhre and K. P. Rykaczewski, *Eur. Phys. J. A*, 2023, **59**, 304.
21 K. R. Singh, V. Nayak, T. Sarkar and R. P. Singh, *RSC Adv.*, 2020, **10**, 27194–27214.
22 S. S. Lee, H. Zhu, E. Q. Contreras, A. Prakash, H. L. Puppala and V. L. Colvin, *Chem. Mater.*, 2012, **24**, 424–432.
23 K. Popa, O. Walter, O. D. Blanco, A. Guiot, D. Bouëxière, J.-Y. Colle, L. Martel, M. Naji and D. Manara, *CrystEngComm*, 2018, **20**, 4614–4622.
24 P.-L. Chen and I.-W. Chen, *J. Am. Ceram. Soc.*, 1993, **76**, 1577–1583.
25 A. Singh, R. Saini, P. Kumar, R. Nongjai, R. C. Meena and K. Asokan, *AIP Conf. Proc.*, 2020, **2220**, 040031.
26 F. Zhang, Q. Jin and S.-W. Chan, *J. Appl. Phys.*, 2004, **95**, 4319–4326.
27 S. Patil, A. Sandberg, E. Heckert, W. Self and S. Seal, *Biomaterials*, 2007, **28**, 4600–4607.
28 J. J. Ketzial and A. S. Nesaraj, *J. Ceram. Process. Res.*, 2011, **12**, 74–79.
29 E. K. Goharshadi, S. Samiee and P. Nancarrow, *J. Colloid Interface Sci.*, 2011, **356**, 473–480.
30 K. Anupriya, E. Vivek and B. Subramanian, *J. Alloys Compd.*, 2014, **590**, 406–410.
31 D. He, H. Hao, D. Chen, J. Lu, L. Zhong, R. Chen, F. Liu, G. Wan, S. He and Y. Luo, *J. Environ. Chem. Eng.*, 2016, **4**, 311–318.
32 J. Calvache-Muñoz, F. A. Prado and J. E. Rodríguez-Páez, *Colloids Surf., A*, 2017, **529**, 146–159.
33 F. Caputo, M. Mameli, A. Sienkiewicz, S. Licoccia, F. Stellacci, L. Ghibelli and E. Traversa, *Sci. Rep.*, 2017, **7**, 4636.
34 I. Y. Habib, N. T. R. N. Kumara, C. M. Lim and A. H. Mahadi, *Solid State Phenom.*, 2018, **278**, 112–120.

35 S. Balaji, B. K. Mandal, L. Vinod Kumar Reddy and D. Sen, *Bioengineering*, 2020, **7**, 26.
36 C. Maria Magdalane, K. Kaviyarasu, B. Siddhardha and G. Ramalingam, *Mater. Today: Proc.*, 2021, **36**, 130–132.
37 A. S. Fudala, W. M. Salih and F. F. Alkazaz, *Mater. Today: Proc.*, 2022, **49**, 2786–2792.
38 W. P. Hsu, L. Ronnquist and E. Matijevic, *Langmuir*, 1988, **4**, 31–37.
39 M. Panahi-Kalamuei, S. Alizadeh, M. Mousavi-Kamazani and M. Salavati-Niasari, *J. Ind. Eng. Chem.*, 2015, **21**, 1301–1305.
40 V. Neck and J. I. Kim, *Solubility and Hydrolysis of Tetravalent Actinides*, Karlsruhe Institute of Technology – Institute for Nuclear Waste Disposal, Karlsruhe, Germany, 1999.
41 J. A. Katalenich, *J. Sol-Gel Sci. Technol.*, 2017, **82**, 654–663.
42 L. Besra and M. Liu, *Prog. Mater. Sci.*, 2007, **52**, 1–61.
43 S. Hu, W. Li, H. Finklea and X. Liu, *Adv. Colloid Interface Sci.*, 2020, **276**, 102102.
44 C. A. Schneider, W. S. Rasband and K. W. Eliceiri, *Nat. Methods*, 2012, **9**, 671–675.
45 C. K. Sio, T. Parsons-Davis, E. Lee, J. Wimpenny, A. J. Pascall, J. D. Kuntz, J. J. Goodell, K. E. Roberts, B. B. Bandong and N. R. Bennett, *Rapid Commun. Mass Spectrom.*, 2020, **34**, e8627.
46 P. S. Boone, S. Harris, C. Ramon, J. Shusterman, A. J. Pascall and T. Parsons-Davis, *Mater. Lett.*, 2024, **361**, 136089.
47 C. F. Holder and R. E. Schaak, *ACS Nano*, 2019, **13**, 7359–7365.
48 J. Stetefeld, S. A. McKenna and T. R. Patel, *Biophys. Rev.*, 2016, **8**, 409–427.
49 Q. Tian and H. Liu, *Nanotechnol.*, 2015, **26**, 175102.
50 S. Thomas, R. Thomas, A. K. Zachariah and R. Kumar, *Thermal and Rheological Measurement Techniques for Nanomaterials Characterization*, Elsevier, 2017.
51 Micromeritics Instrument Corporation, Key Parameters When Using Dynamic Light Scattering, **https://www.azom.com/article.aspx?ArticleID=16772**, accessed November 13, 2023.
52 U. Nobbmann, Intensity-Volume-Number, **https://www.materials-talks.com/intensity-volume-number-which-size-is-correct/**, accessed November 13, 2023.
53 S. Panigrahi, S. Bhattacharjee, L. Besra, B. P. Singh and S. P. Sinha, *J. Eur. Ceram. Soc.*, 2010, **30**, 1097–1103.
54 C. Walkey, S. Das, S. Seal, J. Erlichman, K. Heckman, L. Ghibelli, E. Traversa, J. F. McGinnis and W. T. Self, *Environ. Sci. Nano*, 2015, **2**, 33–53.
55 I. Roger, S. Rau and C. Streb, *ACS Omega*, 2020, **5**, 21250–21253.